International Journal of Multiphase Flow 36 (2010) 249–260

Contents lists available at ScienceDirect

International Journal of Multiphase Flow

journal homepage: www.elsevier.com/locate/ijmulflow

Bubble nucleation characteristics in pool boiling of a wetting liquid on smooth and rough surfaces

John P. McHale, Suresh V. Garimella *

Cooling Technologies Research Center, School of Mechanical Engineering and Birck Nanotechnology Center, Purdue University, West Lafayette, IN 47907-2088, USA

ARTICLE INFO

Article history:
Received 26 October 2009
Received in revised form 30 November 2009
Accepted 7 December 2009
Available online 16 December 2009

Keywords:
Pool boiling
Bubble nucleation
Surface enhancement
Surface roughness

ABSTRACT

Quantitative measurements are obtained from high-speed visualizations of pool boiling at atmospheric pressure from smooth and roughened surfaces, using a perfluorinated hydrocarbon (FC-77) as the working fluid. The boiling surfaces are fabricated from aluminum and prepared by mechanical polishing in the case of the smooth surface, and by electrical discharge machining (EDM) in the case of the roughened surface. The roughness values (R_a) are 0.03 and 5.89 μm for the polished and roughened surfaces, respectively. The bubble diameter at departure, bubble departure frequency, active nucleation site density, and bubble terminal velocity are measured from the monochrome movies, which have been recorded at 8000 frames per second with a digital CCD camera and magnifying lens. Results are compared to predictions from existing models of bubble nucleation behavior in the literature. Wall superheat, heat flux, and heat transfer coefficient are also reported.

1. Introduction

Bubble dynamics in pool boiling have been extensively studied since Lord Rayleigh (1917) first derived an expression for the inertially controlled growth or collapse of vapor bubbles, motivated in part by the sound produced inside a boiling tea kettle. The motivation for successive studies has been the formulation of predictive models for heat transfer in cooling systems for nuclear reactors, refrigeration cycles, and electronics. Roughened or otherwise enhanced surfaces are present in many commercial boiling devices, because of the high active nucleation site densities and consequent increase in boiling heat transfer coefficient they produce. The purpose of the present study is to build upon a previous investigation (Jones et al., 2009), in which pool boiling heat transfer from aluminum surfaces with widely varying R_a values was studied with two fluids, water and FC-77, having significantly different wetting characteristics. The experimental results of Jones et al. (2009) were compared to several heat transfer correlations that incorporate surface roughness effects. For the present work, high-speed visualizations of FC-77 boiling from two of the surfaces were obtained so that the bubble nucleation phenomena could be experimentally characterized in detail.

Four physical mechanisms have been suggested for heat transfer occurring during saturated nucleate boiling: microlayer evaporation (Hsu and Graham, 1961; Hendricks and Sharp, 1964), reflooding transient conduction (Forster and Greif, 1959; Mikic and Rohsenow, 1969b), natural convection (Zuber, 1963; Han and Griffith, 1965), and microconvection (Rohsenow, 1952; Forster and Zuber, 1955; Tien, 1962; Kolev, 1995). Later models (Van Stralen, 1970; Judd and Hwang, 1976; Benjamin and Balakrishnan, 1996), and most recently (Moghaddam and Kiger, 2009) have considered more than one of these mechanisms and obtained a good match with particular sets of data included in the validation.

The following bubble nucleation quantities are usually considered in matching model predictions to experimental observations:

1. Average bubble departure diameter, D_d.
2. Average bubble departure frequency, f_d.
3. Average active nucleation site density, N''_A.

In some instances, the bubble terminal rise velocity $v_{b,term}$ has also been considered in the comparisons. In the present study, these four quantities are measured from high-speed movies of saturated pool boiling of FC-77 from two aluminum surfaces of different roughness at four different heat fluxes to generate a detailed database of experimental results.

Much of the literature has concentrated on boiling from either smooth surfaces or those with geometrically idealized cavities such as v-shaped grooves, conical pits, or reentrant cavities. Consequently bubble nucleation characteristics have not been the subject of many detailed studies for surfaces with more naturally and randomly occurring roughness structures, especially where high nucleation site densities occur. In many previous studies using direct measurements from high-speed movie images, such as those of Wang and Dhir (1993a,b), Pinto et al. (1996), Lee

* Corresponding author. Tel.: +1 765 494 5621.
E-mail address: sureshg@ecn.purdue.edu (S.V. Garimella).

0301-9322/$ - see front matter © 2009 Elsevier Ltd. All rights reserved.
doi:10.1016/j.ijmultiphaseflow.2009.12.004

et al. (2003), and Kim et al. (2006) the bubbles have been relatively isolated from one another. This type of behavior is observed in less wetting fluids, fluids on smooth surfaces, or at low heat fluxes. In other studies, such as those of Abarajith et al. (2004) and Zhang and Shoji (2003), only groups of two to five interacting bubble sites, isolated from other sites on the surface by design, were observed or simulated for the sake of simplicity and to model the specific types of bubble interactions which might occur on the surface. Bubble nucleation interactions may also occur due to thermal diffusion in a conductive substrate, as shown by Chekanov (1977) and Sultan and Judd (1983), although these authors concluded opposite effects. Chekanov found that nucleation at neighboring sites were suppressed by a dominant site, while Sultan and Judd showed that bubble nucleation at one site could produce a wave of high temperature that augmented nucleation at neighboring sites.

Several previous studies have investigated the effect of surface roughness on pool boiling heat transfer. Recently, Kotthoff and Gorenflo (2009) studied the effects of surface roughness and tube diameter on nucleation site density and heat transfer coefficient in pool boiling of various refrigerants and organic liquids from copper tubes. They confirmed previous findings (Gorenflo et al., 2004) that active site densities integrated over time are higher than those apparent over only a few ebullition periods. Together with the surface analysis described by Luke (2009), they concluded that surface roughness descriptions based upon height parameters cannot be used to accurately predict the influence of surface roughness on boiling heat transfer. The works of Luke et al. (Luke et al., 2000; Luke, 2003, 2009) and an earlier study by Bier et al. (1979) calculated cavity sizes from profilometer scan data to predict potential nucleation site size distributions for their surfaces. These and similar studies have linked the surface roughness effect to nucleation site density alone without considering bubble dynamics in detail.

Other studies have shown that surface roughness may affect both static and dynamic contact angles, and have linked this effect to various aspects of bubble nucleation and boiling heat transfer. The early correlation of Fritz (1935), based on a static force balance, relates bubble departure diameter to be in direct proportion to the apparent contact angle. Cornwell (1982) produced a geometric argument for differing values of advancing and receding contact angles on rough surfaces. Tong et al. (1990) summarized the measured values of static contact angle reported in the literature for highly wetting liquids on a variety of surfaces, and then explored the effects of contact angle on boiling incipience. Hong et al. (1994) observed a decrease in static contact angles of water, refrigerants, and alcohols on metal surfaces of increasing roughness and/or degree of oxidation. Bernardin et al. (1997) summarized different definitions for contact angle and tabulated values of advancing contact angle for water on metals with different surface preparation methods, showing the wide range of reported values. Kandlikar and Steinke (2001) examined the effects of copper and stainless steel surface roughness on static, advancing, and receding contact angles of water droplets. They found that values for all three types of contact angle decreased with surface roughness for stainless steel, but first decreased, then increased with increasing surface roughness for copper. Hibiki and Ishii (2003) correlated active nucleation site density with static contact angle, obtaining very good agreement with their model for a wide variety of liquids and test conditions. Lorenz et al. (1974), and Qi and Klausner (2005) demonstrated geometric arguments showing that cavity size and shape, static, and dynamic contact angle can affect the filling and/or vapor-trapping capabilities of nucleation sites. Hazi and Markus (2009) showed through Lattice-Boltzmann simulations that bubble departure frequency, but not the bubble departure diameter, in pool boiling of a water-like fluid was greatly changed by varying the static contact angle parameter. Despite a large amount of data in the literature on the subject, reasons for these contact angle behaviors are still elusive, and a number of authors (Kandlikar and Steinke, 2002; Hibiki and Ishii, 2003) have recommended further study of surface roughness and fluid wetting effects.

In the present study, which expands on preliminary results presented by McHale and Garimella (2008), one smooth surface and one very rough surface producing a high active nucleation site density were included in the testing. In addition, the heat flux was varied over a wide range, approaching the critical heat flux. As a result, bubble interactions and mergers occurred frequently and randomly. The effects of surface roughness and wall superheat on the bubble nucleation parameters are explored. Measurements of the dynamic contact angle θ for growing FC-77 bubbles on aluminum are also reported; to the authors' knowledge, such measurements have not been previously reported in the literature.

2. Experimental setup

A schematic diagram of the test setup, which was modified from that used by Jones et al. (2009), is shown in Fig. 1. Each test piece consisted of an aluminum block into which twelve 3.18-mm diameter cartridge heaters were inserted in a distribution (Fig. 1b) that ensured a uniform heat flux at the top of the test surface. Six 0.81-mm diameter thermocouples were positioned in the upper portion of the block, arranged in two horizontal rows separated by a 3.18-mm gap, so that the temperature of the surface T_w could be obtained by extrapolation. Aluminum silicate insulation was

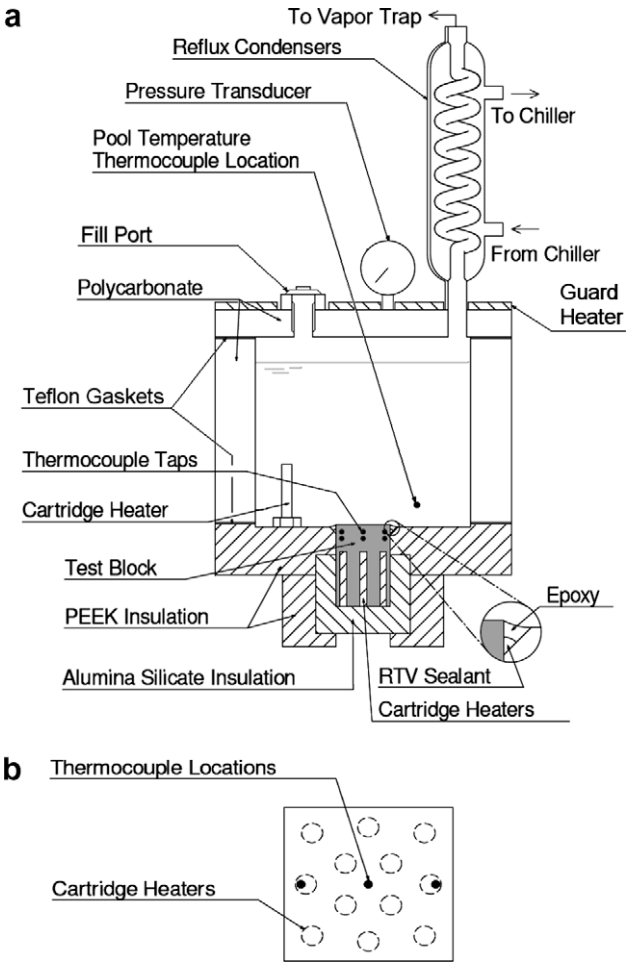

Fig. 1. (a) Schematic diagram of the experimental facility with relevant components indicated and (b) top view of the test block.

placed around the heated portion of the block and was in turn surrounded by additional PEEK insulation ($k \approx 0.28$ W/m K). The power input to the cartridge heaters was measured. A numerical model was used to estimate the heat loss from the block, which was subtracted from the total power input to arrive at the heat flux q''_w through the top surface.

The bottom of the test chamber was also made of PEEK, and the test block was inserted into this base. The insertion gap (inset, Fig. 1a) surrounding the 25.4-mm square test piece was filled with a high-temperature RTV silicone caulk. The remaining trough was filled with a low-viscosity epoxy. This procedure prevented leakage from the pool, while at the same time avoiding the formation of unwanted nucleation sites on the sides of the aluminum block; the epoxy also prevented exposure of the Fluorinert fluid to extractable chemical species in the RTV.

The sides of the chamber were built from individual sheets of polycarbonate joined and leak-proofed at the corners. The back and side walls, which were not required to be transparent, were then covered with additional silicone foam insulation to minimize heat losses from the chamber. The top and bottom of the chamber were sealed with thin Teflon gaskets. The top wall of the chamber was made from a fiber–epoxy composite, G-11. A heated aluminum plate maintained at the liquid saturation temperature was placed on top of the G-11 sheet, effectively minimizing heat loss through the top wall of the chamber.

Inserted into the top wall were a fill port with a funnel and two Pyrex Graham-type condensers cooled by water at approximately 28 °C from a chiller. In order to ensure the retention of all FC-77 vapor, the tops of the condensers vented to atmosphere through a cold vapor trap maintained at 0 °C. The pool and chamber were thus maintained at atmospheric pressure, as verified with a pressure transducer.

Two immersion-type cartridge heaters were located in the lower part of the pool to maintain the pool at saturation temperature T_{sat}, a condition that was verified by thermocouples located at the bottom and in the middle of the pool. The saturation temperature of the fluid was determined by heating the pool until the temperature measured with the thermocouples reached a constant maximum value. The power input to the pool heaters was then decreased to the minimum value necessary to maintain the pool at the saturation temperature. The experimentally measured saturation temperature for FC-77 was consistently between 100.1 and 100.5 °C. The saturation temperature of different batches of FC-77 lies in the range of 97–101 °C, according to the manufacturer (3 M). The setup was operated for periods of up to 70 h continuously, with the only loss of fluid occurring during filling and draining.

Two test pieces used earlier by (Jones et al., 2009) were chosen for further study here: the smooth surface with an average roughness R_a value of 0.03 μm produced by mechanical polishing using progressively finer grades of sandpaper, and the electrical discharge machined (EDM) surface with an R_a value of 5.89 μm.

High-speed movies of boiling from the surface were recorded using a Photron Fastcam Ultima APX grayscale digital camera at 8000 frames per second, illuminated from the side by a light sheet from a green solid-state laser (532 nm wavelength). After the field width of the video frame was calibrated with the camera focused on a scale located in front of the test surface, the camera was translated forward via a micrometer-driven stage until the front portion of the test piece was in focus. The focus and zoom of the lens remained constant to ensure an unchanged image width. A diagram illustrating the illumination and camera placement is given in Fig. 2.

Results of the heat transfer measurements for all five surfaces tested by Jones et al. (2009) with FC-77 as the boiling fluid are shown in Fig. 3 for reference. The critical heat flux (CHF) was reached in three of the trials, and is denoted by an ×. EDM-roughening of the surface to 1.0 μm R_a decreased the wall superheat, increased the heat transfer coefficient, and increased CHF. Higher

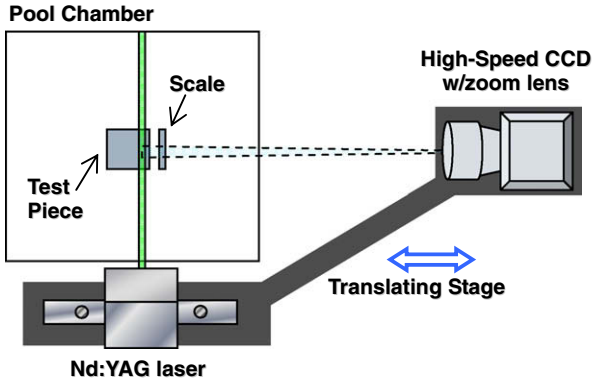

Fig. 2. Illumination and scale calibration scheme.

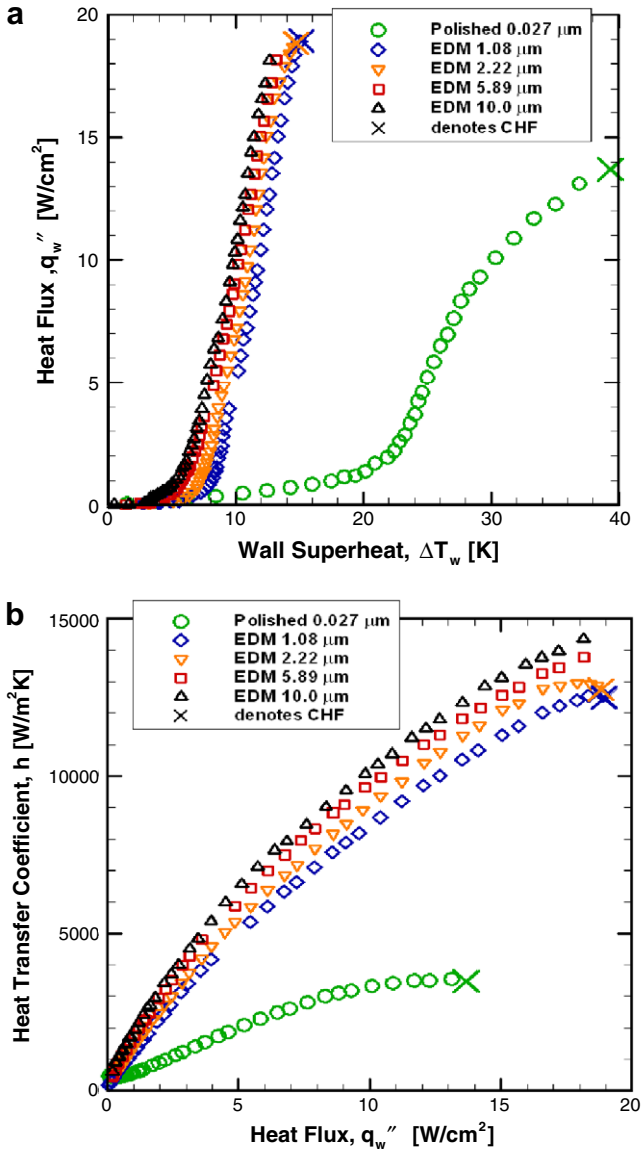

Fig. 3. Boiling curves for FC-77 on five surfaces of varying roughness: (a) heat flux versus wall superheat and (b) heat transfer coefficient versus heat flux, after (Jones et al., 2009).

roughness values further decreased the wall superheat ΔT_w and increased the heat transfer coefficient slightly.

3. Qualitative observations

Still images of boiling on the two surfaces are shown in Fig. 4 for four heat fluxes. From the top row to the bottom row, the heat flux at the wall increases from approximately 2 W/cm^2 up to 11 W/cm^2. Bubbles nucleate and grow while still attached to the test surface (located at the bottom of the frame), and then detach under the influence of buoyancy, quickly moving up out of the field of view. What may be termed the *bubble interaction layer*, i.e., a region of interaction between bubbles attached to or only recently detached from the surface, is visible in the bottom quarter of the frame.

Several differences are apparent in the nucleation behavior of bubbles on the polished and roughened surfaces (left and right set of panels, respectively in Fig. 4). First, far fewer active nucleation sites are observed for the polished surface at the lower heat fluxes, as shown in the upper left image of Fig. 4. Bubbles appear to be generally isolated from neighboring sites during much of the growth period, and grow to a relatively large size before merging or detaching. *Consecutive-pair* bubbles occur when a single site spawns a bubble embryo which remains attached to the surface but slides away from the cavity in the direction of induced bulk flow, while continuing to grow. Another bubble then originates from the same site, but grows quickly enough for its surface to intercept the larger sliding bubble. The small bubble attached to the nucleation site is then removed in a merger with the first, larger bubble. Small growing embryos continue to be formed and swallowed by the first bubble until it moves far enough away to preclude any interaction with its originating site, contributing to an overall periodic nucleating behavior. Four consecutive bubbles sliding from the same nucleating site are shown while still attached to the polished surface in Fig. 5. In measurements, the detachment is considered to occur when the first bubble actually

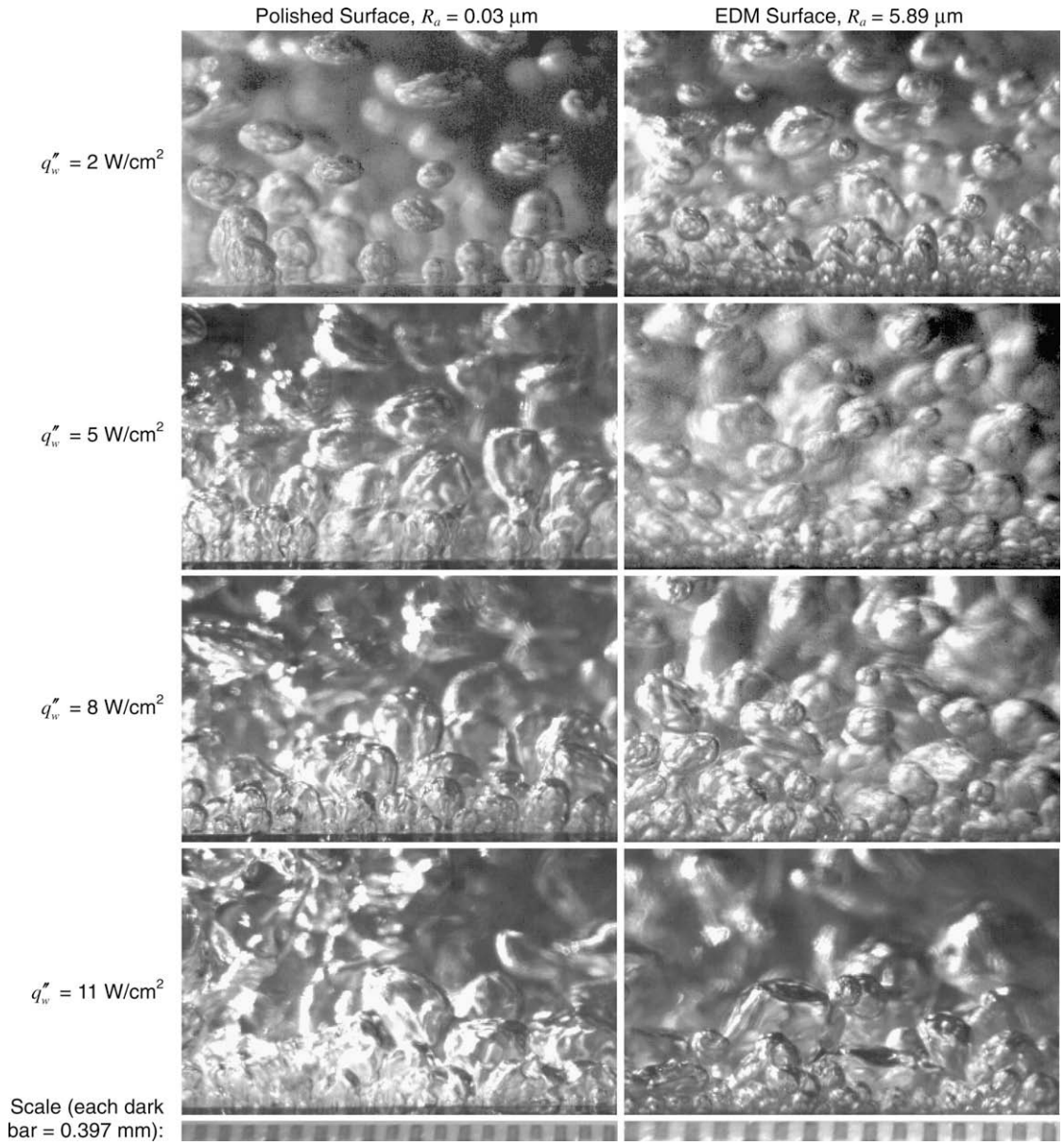

Fig. 4. Images obtained at 8000 frames per second depicting the effect of surface roughness and heat flux upon the nucleation behavior of vapor bubbles on a heated wall. The scale is shown below the photos.

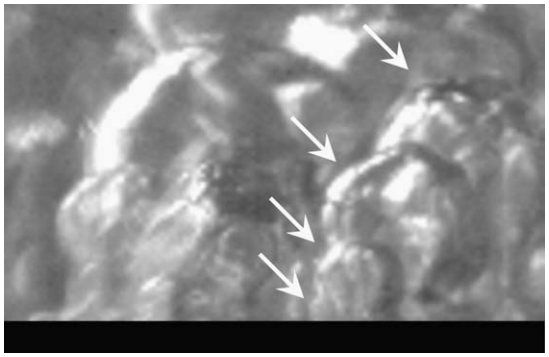

Fig. 5. Four distinct bubbles originating from the same nucleation site still attached and sliding along the surface.

breaks off from the surface rather than when the final separation from the nucleating site is apparent.

In contrast to the polished surface behavior, no periodic behavior is exhibited with the roughened surface, shown in the second column of Fig. 4. Bubbles are seldom isolated for much of the growth cycle, and the active site densities are considerably higher. A small embryo grows until it becomes large enough to interfere with other growing or already released bubbles, at which point it either captures the other bubble or is removed from its site by the other. Often, multiple mergers of this kind occur simultaneously, that is, within the time increment of a single frame (1.25×10^{-4} s). The types of mergers classified by Zhang and Shoji (2003) essentially described the mergers observed here: vertical coalescence, horizontal coalescence, and "declining" coalescence. However, declining coalescence seems to dominate for higher heat fluxes, having the effect of keeping large bubbles in or near the bubble layer for an extended time following their departure from the surface. Large bubbles appear to move slowly upward through the bubble layer and are typically subject to several declining coalescence mergers before breaking into a free ascent.

For low to moderate fluxes, bubbles ascend in a mostly isolated fashion. For higher fluxes, e.g., the bottom row in Fig. 4, free bubbles in the bubble layer are pushed into the unsteady vapor/bubble column that forms over the center of the test piece. The vapor column at high heat fluxes and the buoyancy-induced flow region for low to moderate fluxes have a shape similar to an inverted stagnation flow over the whole surface.

The average number of nucleation sites involved in the production of a single large bubble rising into the central buoyant column appears to increase with heat flux. In the bottom two rows of Fig. 4, large bubbles may be seen in the bubble interaction layer, created by the mergers of many smaller bubbles nucleating at sites on the surface. The central buoyant column to which these large bubbles are being drawn is located behind the field of view in focus. For smaller fluxes, mergers are common between two bubbles originating from nucleation sites located within a few diameters (<1 mm) of each other. For higher fluxes, however, mergers occur between bubbles which nucleate from sites at a separation distance of nearly half the image frame, or up to 3 mm. And for the highest flux, nearly all bubbles across the entire width of the heated surface appear to be drawn into a merger with the central vapor column. The main effect of the increased bubble size resulting from more associated nucleation sites is the enhancement of the physical stripping of growing bubbles from the surface, whereupon liquid is pulled in, cooling the vacant site by advection of fluid that is at the saturation temperature, which is then evaporated into a new bubble.

4. Measurement techniques

For many of the test conditions in this work, bubble nucleation parameters were not clearly measurable according to traditional concepts of bubble ebullition, due to the much greater density of nucleation sites on the practical surfaces considered in this work. Specific definitions are therefore provided for the bubble measurements presented. For example, the precise timing of bubble departure events was not readily apparent, as the growing embryos often moved from their nucleation sites while still being attached to the surface, either by merger with a larger neighboring bubble or by sliding due to a buoyancy-driven bulk flow. For some time even upon release from the surface, bubbles often continued to interact with bubbles on the surface before breaking into a free ascent. The interactions appeared to occur randomly, and did not exhibit any patterns or periodicity to their behavior. As a result, it was necessary to collect measurement data over several bubbles for each test case and to report results averaged over many occurrences. Each quantity of interest is reported as an average of the values obtained for at least 25 bubbles per test case.

Five consecutive bubbles from each of five individual nucleation sites identified on the surface in the images were tracked from initiation of growth to the time they disappeared from the image frame. The pixel locations on diametrical points of each bubble were manually determined and logged through hundreds of frames of video, as depicted in Fig. 6. The apparent bubble centroid location in each frame was then calculated as the average of the diametrical x- and y-coordinates. In general, the bubble did not

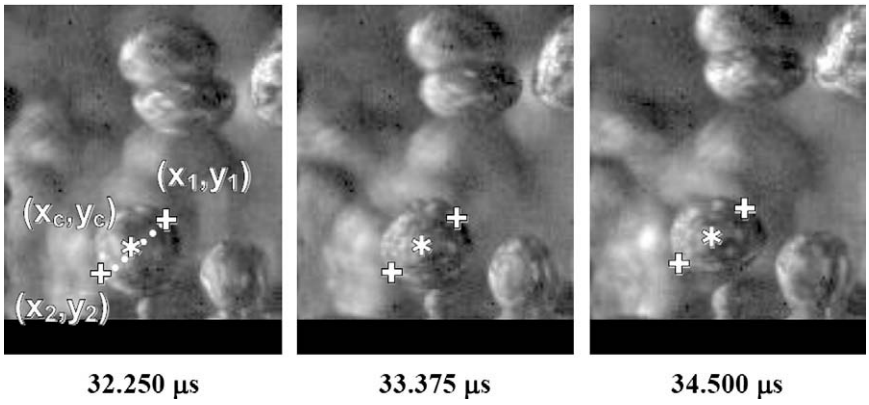

Fig. 6. Illustration of bubble measurement technique showing diametrical points logged (+) and the calculated centroid location (∗) of a bubble produced on the polished surface at 2.06 W/cm^2.

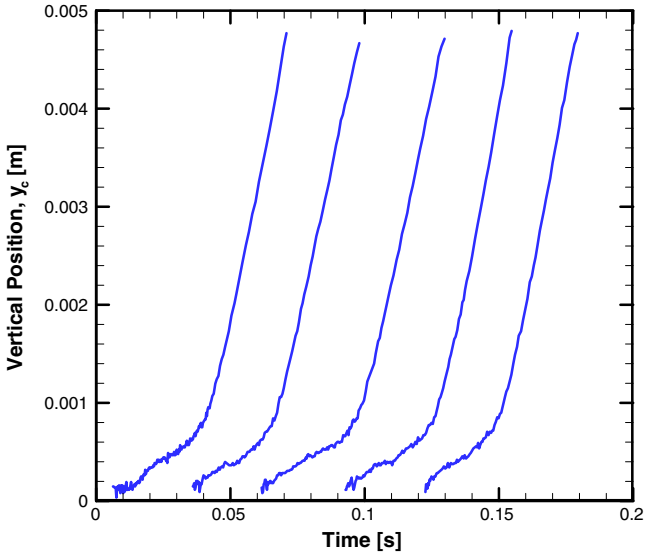

Fig. 7. Time history of the vertical position of five consecutive bubbles originating from a single active nucleation site on the polished surface at 2.06 W/cm^2.

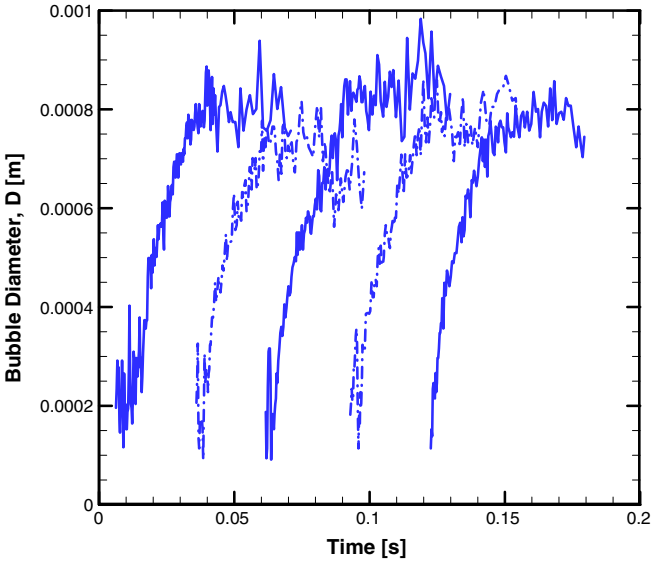

Fig. 9. Growth of five consecutive bubbles originating from a single active nucleation site on the polished surface at 2.06 W/cm^2.

significantly change in position or shape in every consecutive frame; instead, the bubble measurements were made every few frames over which period a measurable change was observed. The bubble diameter and x–y location of its centroid were thus known as a function of time for each bubble.

The pixel resolution was 22.9 μm for the polished (0.03 μm R_a) surface and 18.3 μm for the EDM-roughened (5.89 μm R_a) surface. The y- and x-positions of the centroid and diameters D over time of five bubbles originating from a single nucleation site on the polished surface at a heat flux of 2.06 W/cm^2 are shown in Fig. 7 through 9, respectively. In Fig. 7 the periodicity of the bubble growth and rise process is apparent for boiling on the polished surface at a low heat flux. In Fig. 8 it may be seen that bulk flow is responsible for moving the bubbles horizontally following departure. Fig. 9 again illustrates the periodic nature of boiling for this test condition and gives a sense for the magnitude of noise (up to ±10%) inherent in these two-point measurement data.

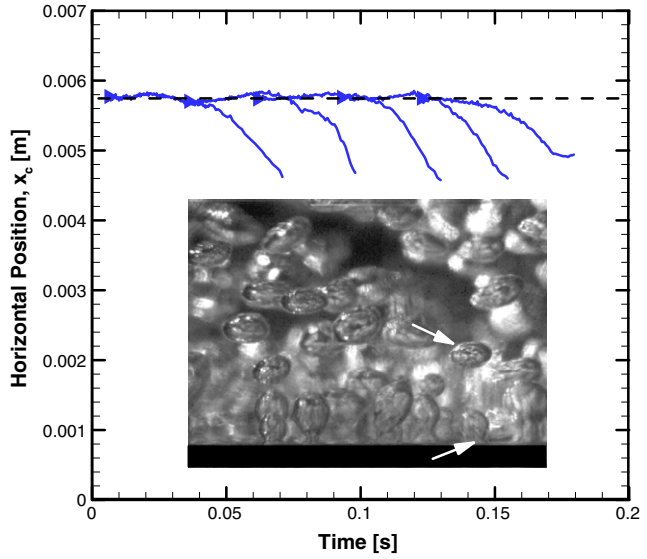

Fig. 8. Time history of the horizontal position of five consecutive bubbles originating from a single active nucleation site on the polished surface at 2.06 W/cm^2. Two of these bubbles are indicated by arrows in the inset photograph. Triangular symbols denote the initiation of bubble growth.

4.1. Bubble departure frequency

The bubble departure frequency could be estimated by one of two methods: the difference in time between successive initiations of bubble growth at a single nucleation site, as suggested by Darby (1964), or the time elapsed between apparent departure events. A departure event was difficult to identify precisely for reasons described above, but could be approximated from the time history of the vertical position of the bubble centroid. A constant radial growth rate was assumed, which is a reasonable approximation for much of the growth period according to Lord Rayleigh (1917), Mikic et al. (1970), and others. For an attached bubble, the constant radial growth rate assumption results in a linear change in bubble centroid position with time. Straight lines were fit to the growth portion and free ascent portions in the curve, as shown in Fig. 10, where the start of the time scale is arbitrary. The intersection of the growth line with the x-axis is a good estimate of the initiation point, while the intersection of the growth and free ascent lines is considered a good estimate of the point of departure.

The bubble shown in Fig. 10 was modeled as a body rising freely under the action of buoyancy and drag forces to investigate the importance of acceleration:

$$\begin{aligned} &\ddot{y} + \tfrac{3}{4}\tfrac{\rho_l C_D}{\rho_v D}\dot{y}^2 = \tfrac{(\rho_l-\rho_v)g}{\rho_v} \\ &y(t_0) = y_c|_{t=t_0} \\ &\dot{y}(t_0) = \dot{y}_c|_{t=t_0} \end{aligned} \tag{1}$$

where y is the vertical position of the bubble centroid, t_0 the time of departure, C_D the drag coefficient of a spherical bubble, ρ_l and ρ_v are densities of liquid and vapor phases, respectively, and g is acceleration due to gravity. C_D values ranging from 0.14 to 1.22, from the correlations of Michaelides (2003) and Ishii and Zuber (1979), respectively, were used in the analysis. The distance over which a freely accelerating bubble would reach 99% of its terminal velocity (approximately 30–120 μm) was determined to be less than the experimental noise (±3 standard deviations or approximately 200 μm) about the straight-line fit in Fig. 10. A third curve fit

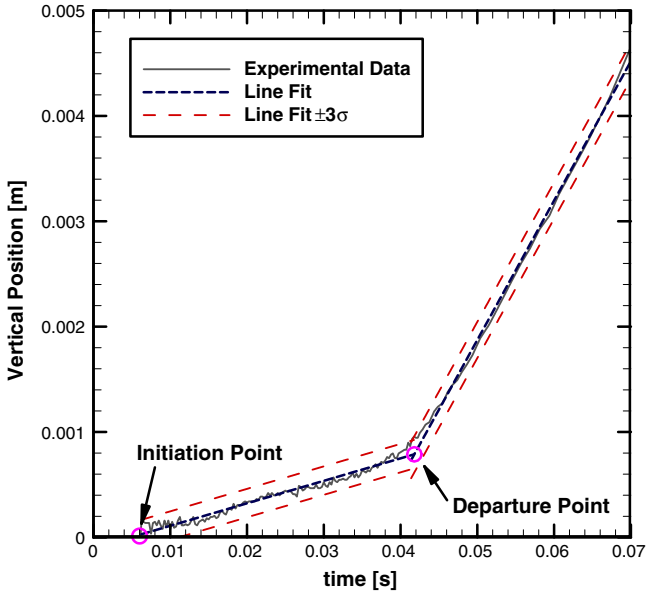

Fig. 10. Illustration of the calculation procedure for bubble initiation and departure times, by analysis of the vertical position of the bubble over time (polished surface at 2.06 W/cm^2).

segment incorporating acceleration effects was therefore considered unnecessary.

Due to bubble interactions following the initiation of growth, bubble initiation frequency f_i was found to have a much lower standard deviation than apparent bubble departure frequency $f_{d,app}$; thus it is assumed that f_i is a higher-confidence estimate of the true mean bubble departure frequency f_d than is $f_{d,app}$. The uncertainty in departure frequency is estimated to be up to 10%.

4.2. Bubble departure diameter

The bubble departure diameter was calculated as an average of diameter measurements within ±5 frames of the calculated departure time for each bubble. It can be seen in Fig. 9 that the diameter measurements obtained from the images can be subject to a considerable amount of scatter, representing a measurement uncertainty of up to 15%. The scatter is primarily due to the manual process of measuring oscillating non-spherical bubbles, especially in the case of large bubbles. The reported diameter measurements are based on best approximations of equivalent diameter in the plane of view.

At high heat fluxes, bubble coalescences or other interactions caused extreme changes in measured diameters and trajectories over the course of a few measurement time steps. These changes obscured the definitions of the key descriptors, "departure diameter" and "terminal velocity". For some bubbles measured, therefore, D_d and $v_{b,term}$ values could not be calculated.

In general, bubble departures were observed to occur when the bubble centroids were located approximately $1.35 \cdot D_b/2$ above the surface, indicating the extent of oblong stretching of a bubble into a balloon shape just prior to departure. This approximate value was independent of heat flux and surface roughness for all test cases in the present study and was a useful estimator of the point of departure when straight lines could not be accurately fit to the growth and/or ascent phases of the bubble-rise trajectories.

4.3. Active nucleation site density

Each movie was also analyzed to determine the locations of the active nucleation sites on the portion of the test piece which was in focus. The instantaneous number of active sites $N_{A,i}$ captured by a still frame was generally not as high as the total, cumulative number of sites $N_{A,cum}$ that were active at least once over several departure periods (Pinto et al., 1996; Gorenflo et al., 2004). Therefore five frames chosen arbitrarily, representing a time increment much greater than one bubble departure period, were studied in detail using the pixel-logging technique described earlier. The number of nucleation sites logged in each frame was averaged to determine the instantaneous number of active nucleation sites. A set of all sites active in any of the five frames was compiled using a tolerance of ±3 pixels in the manual location of the cavity. The criterion, however, did not prevent sites within 3 pixels of each other from being retained if they were visible in the same frame.

The area of the surface included in the analysis was known from the scale in the lateral and depth directions. The area density of active nucleation sites N''_A was then calculated by dividing the counted number of active sites N_A by the calculated area A of the surface in the image. The uncertainty in the measurement is estimated to be 20% for low heat fluxes and up to 40% for high heat fluxes where the field of view was frequently obstructed.

4.4. Terminal velocity

The bubble terminal velocity $v_{b,term}$ was calculated from a straight-line fit to the rise portion of the vertical position measurements. In the example illustrated in Fig. 10, the terminal velocity was determined without further calculation from the slope of this line. Uncertainties associated with the fitting ranged from 2% for low heat fluxes to as much as 50% for the highest heat flux due to coalescences or other changes in bubble trajectory.

5. Results

The test matrix used in the experiments is given in Table 1. Input power to the test pieces was fixed for the four cases at 20 W, 40 W, 60 W, and 80 W, respectively. The measurements therefore correspond to heat-flux controlled pool boiling. The reported heat fluxes in Table 1 are based on the heat input corrected for heat losses. The difference in heat fluxes between the two test pieces is due primarily to differences in heat loss due to higher heat transfer coefficients and a higher thermal conductivity of the block material of the EDM-roughened surface (230 versus 167 W/m K for the polished surface) as described in Jones and Garimella (2007) and Jones et al. (2009).

The properties of FC-77 used in all the calculations are provided in Table 2. The values in Table 2 were obtained from data published by 3M Corporation (1986, 2000), with the exception of vapor density ρ_v and dynamic contact angle θ. The vapor density was unavailable in the literature and was therefore calculated according to the ideal-gas relation. The dynamic contact angle was measured directly from images of isolated bubbles forming on the polished surface in test case 1. The reported value of 0.854 radians

Table 1
Test matrix.

Heat flux, q''_w (W/cm^2)	Wall superheat, $T_w - T_{sat}$ (K)	Surface roughness, R_a (μm)
2.06	16.6	0.03
5.04	18.8	0.03
8.13	20.9	0.03
11.05	25.3	0.03
2.24	6.0	5.89
5.23	7.4	5.89
8.35	8.5	5.89
11.34	9.4	5.89

Table 2
Properties of FC-77 at saturation (3M Corporation, 1986, 2000) and other experimentally determined quantities.

Quantity	Value	Units
T_{sat}	100.1–100.5	(°C)
P	101,325	(Pa)
ρ_l	1592	(kg/m^3)
ρ_v	14.7	(kg/m^3)
μ_l	0.000442	(kg/m s)
$c_{p,l}$	1170	(J/kg K)
k_l	0.057	(W/m K)
α_l	3.06×10^{-8}	(m^2/s)
h_{lv}	89,000	(J/kg)
g	9.81	(m/s^2)
θ	0.854	(radians)
σ	0.0057	(N/m)
Pr_l	9.08	–
T_{crit}	495	(K)
P_{crit}	1.58×10^6	(Pa)
M	416	(kg/kmol)
Ja	8.56–36.06	–

was the average of measurements of 20 different bubbles, with a standard deviation of 0.076 radians. Twelve measurements of dynamic contact angle for the EDM-roughened surface were statistically indistinguishable from the polished-surface values.

The variation of Jakob number Ja, defined as $(T_w - T_{sat})c_{p,l}\rho_l/\rho_v h_{lv}$, is shown in Fig. 11. A power-law fit is shown as dashed lines to assess the standard assumption of the dependence between heat flux and wall superheat. Since a precise relationship with either heat flux or wall superheat has not been shown for many of the nucleation quantities, this figure may be of use in interpreting the figures that follow, which use Ja as the independent variable.

5.1. Departure diameter

The average departure diameters for each case, shown in Fig. 12, were compared to correlations for departure diameter given by Fritz (1935), Ruckenstein (1961), Cole and Shulman (1966), Hatton and Hall (1966), Cole (1967), Cole and Rohsenow (1969), Kutateladze and Gogonin (1980), Borishanskiy et al. (1981), Jensen and Memmel (1986), and Lee et al. (2003). The experimentally measured departure diameters increased with heat flux and wall superheat for each surface. The standard deviations were on average 26% of the measured values; the distribution of departure diameters is therefore wide. As may be seen in the figure, the effect of surface roughness on bubble departure diameter is not due to wall superheat alone. Although the correlations rightly predict an increase in D_d with Ja, the experimental data do not suggest a single curve independent of roughness. The departure diameters for the rough surface are smaller for a given heat flux, but are larger for a given value of Ja, relative to the polished surface. The measured contact angle of 0.854 radians, which did not significantly change for different surface and heat flux conditions, was used in calculating results from several of the correlations. Of the correlations considered, only that of Hatton and Hall (1966) includes direct consideration of surface conditions. The effect of cavity size under their analysis, however, is negligible for the FC-77 boiling system studied here since drag and inertial force terms dominate the dynamic force balance for a low surface tension, wetting fluid. Also, for a power-controlled surface, none of the available correlations are fully predictive, since the wall superheat inherent in Ja must be obtained from the experimentally determined q–T boiling curve.

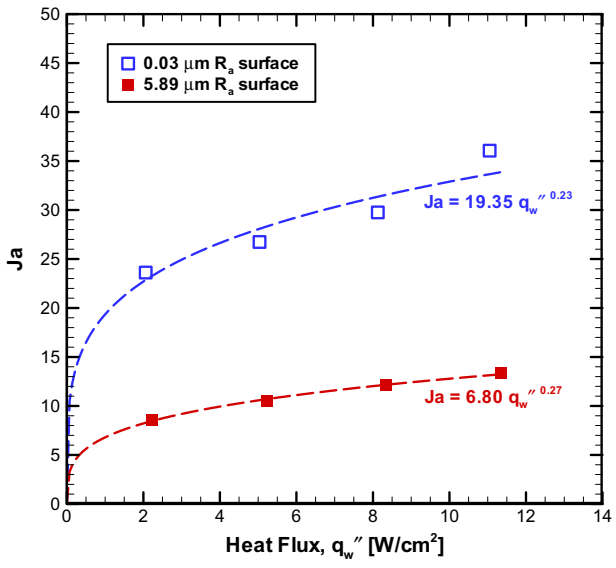

Fig. 11. Variation of Jakob number with heat flux applied at the surface.

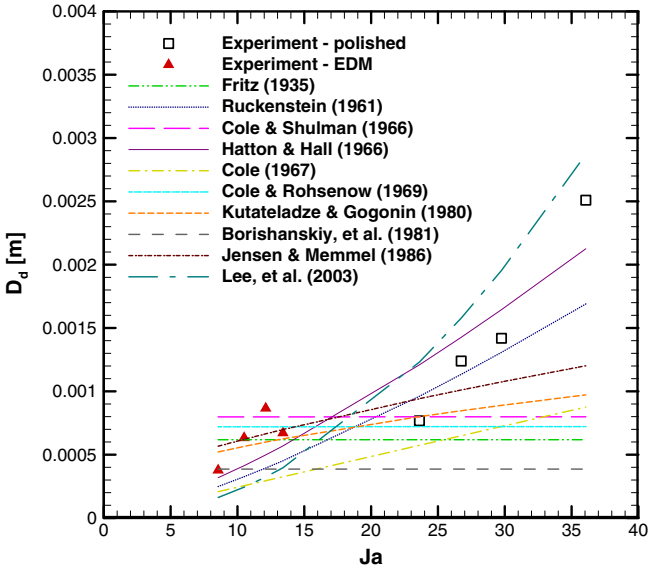

Fig. 12. Variation of bubble diameter at apparent departure with Ja for the two surfaces. Experimental data are compared with predictions from selected correlations from the literature, based on the measured θ of 0.854 radians.

5.2. Departure frequency

The measured bubble departure frequencies are plotted with respect to Ja in Fig. 13a. As for departure diameter, the experimental frequency data do not show a single relationship with wall superheat or with heat flux. Values of f for the polished surface are lower than for the roughened surface by as much as 47% for a given heat flux, with less difference at higher heat fluxes. In Fig. 13b, the measured bubble departure frequencies are plotted as their product with departure diameter (fD_d) versus Ja. Fig. 13c similarly shows the product of the square root of frequency and the diameter $\left(f^{\frac{1}{2}}D_d\right)$, as this quantity is used in the correlation of Mikic and Rohsenow (1969a). These experimental results are compared to predictions from several correlations:

Jakob and Fritz (1931):

$$fD_d = 0.078 \tag{2}$$

Peebles and Garber (1953):

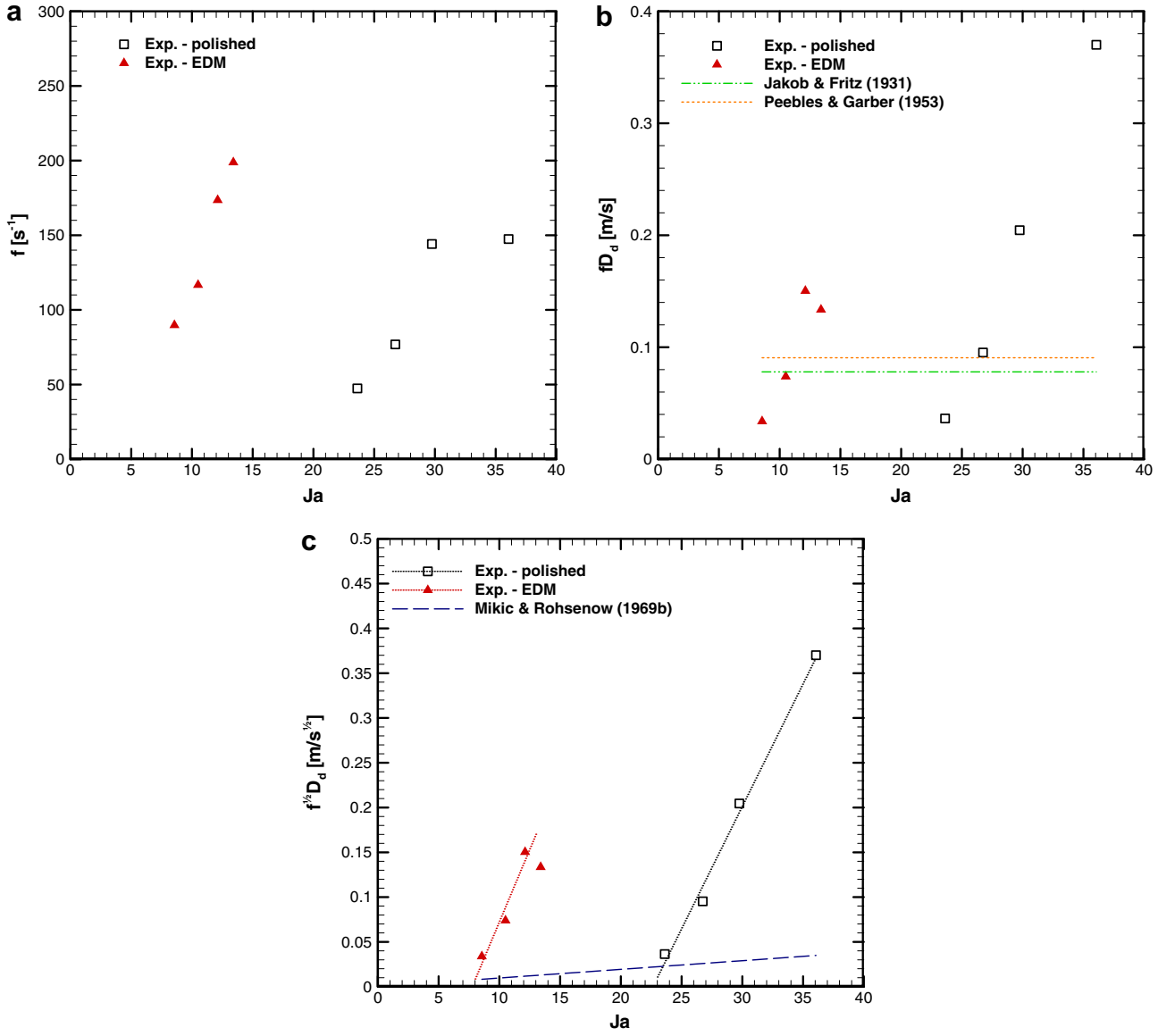

Fig. 13. Measured bubble departure (a) frequency, (b) frequency–diameter product, and (c) root-frequency–diameter product, compared with some commonly used correlations.

$$fD_d = 1.18\left(\frac{t_g}{t_g + t_w}\right)\left(\frac{\sigma g(\rho_l - \rho_v)}{\rho_l^2}\right)^{0.25} \tag{3}$$

and Mikic and Rohsenow (1969a):

$$f^{\frac{1}{2}}D_d = \left(\frac{4}{\pi}\right)Ja\sqrt{3\pi\alpha_l}\left[\left(\frac{t_g}{t_g + t_w}\right)^{\frac{1}{2}} + \left(1 + \frac{t_g}{t_g + t_w}\right)^{\frac{1}{2}} - 1\right], \tag{4}$$

in which the ratio of the time period for bubble growth to the time period for a complete ebullition cycle is $t_g/(t_g + t_w)$, where t_g is the average time required for bubble growth at a test condition, measured in seconds, and t_w is the average waiting period in seconds for a test condition, i.e., the average time required for another embryo to appear at any specific site after a bubble release event. The waiting periods t_w ranged from 0 to 9 ms. None of the correlations match the trends found in the experimental data. Eq. (2) may account for the effects of surface roughness, heat flux, or wall superheat on *either* D_d *or* f, but implies that an inverse relationship between ebullition frequency and departure diameter keeps the product of the two constant, regardless of other conditions. Eq. (3) includes these quantities, but only insofar as they affect the ratio of growth period to bubbling period, while Eq. (4) also accounts for wall superheat relation in terms of *Ja*. Eq. (2) was developed based on experimental data from the pool boiling of water and liquid hydrogen, while Eqs. (3) and (4) were developed through theoretical arguments.

None of the departure frequency correlations seem applicable to the pool boiling of a Fluorinert and do not capture the trends seen in the experimental data, although the orders of magnitude (100 s^{-1}) are comparable. In the present experiments, both bubble departure frequency and diameter were seen to increase with heat flux; this increase was much more pronounced for the polished surface. It can be argued from Figs. 12 and 13 that the rough surface is generally more effective at evaporating fluid, producing higher D_d and fD_d for a given thermal potential, *Ja*.

5.3. Nucleation site density

The active nucleation site densities are shown in Fig. 14, and are compared with the predictions from Benjamin and Balakrishnan (1996) and Hibiki and Ishii (2003). The number of active sites increased with increasing wall superheat and with increasing surface

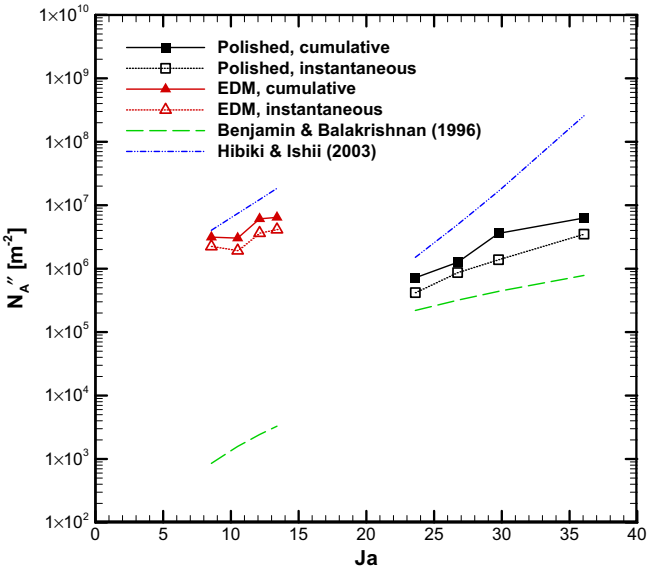

Fig. 14. Active nucleation site densities for the polished and rough surfaces as a function of Jakob number. Instantaneous active site density is shown with open symbols and dotted connectors, while cumulative active site density is shown with filled symbols and solid connectors.

roughness. The instantaneously active nucleation site densities were on average 52.1% and 63.8% of the cumulative active site densities (as discussed in Section 4.3) for the polished and roughened surfaces, respectively. The percent difference in measured cumulative active nucleation site densities between the two surfaces varied from 77.1% for the lowest heat flux to less than 3% for the highest. The polished surface exhibited a full order-of-magnitude increase in active site density from the lowest heat flux to the highest, while the roughened surface exhibited only half this increase. By comparing Figs. 3 and 14, it may be seen that the relatively shallow slope of the boiling curve for the polished surface in Fig. 3 coincides with a wide range of *Ja* in Fig. 14. The difference in the boiling curves in Fig. 3 may be partly explained by a wider range of (and generally higher) superheats necessary to sustain active nucleating cavities on the polished surface according to Hsu's (1962) criterion. At low heat fluxes, the bubble departure diameters for the two surfaces are similar, as shown in Sections 5.1 and 5.2, despite very different active site densities. At high heat fluxes, however, the active site densities and ebullition frequencies for the two surfaces are similar, but the bubble departure diameters are significantly larger for the polished surface. It is difficult to determine from these data whether differences in bubble departure diameters and frequencies for the two surfaces are also causes for differences in the boiling curve, or whether they are merely related effects, or indeed, whether any simple relationship could even be deduced.

The correlation of Hibiki and Ishii (2003) is semi-empirical, having been fit to a wide array of experimental nucleation site density data for boiling from primarily smooth surfaces. They assumed that nucleating cavity number and size distributions would be statistically similar for most boiling systems, accounting for surface characteristics by including a static contact angle term. The predictions plotted in Fig. 14 are for static contact angles of 0.1 and 0 radians for FC-77 on the polished and roughened surfaces, respectively. These values are merely estimates based on the wetting behavior of FC-77 on the aluminum surfaces, since static contact angles could not be determined from the high-speed movies. Overall, agreement between the Hibiki–Ishii correlation and the experiments is reasonable if suitable values of θ are used. The correlation using the estimated values of static contact angle slightly overpredicts the measured values.

The correlation of Benjamin and Balakrishnan (1996) implies an inverse relationship between R_a and N''_A for systems in which the parameter R_aP/σ is greater than approximately six. Since it is generally agreed that increased roughness leads to an increase in number of nucleating cavities on the surface, the EDM-roughened surface ($R_aP/\sigma > 100$) is well outside the scope of their correlation. Agreement with the present experimental data for the polished surface is as good as the Hibiki–Ishii correlation, but the measurements are underpredicted.

5.4. Terminal rise velocity

The terminal velocities of the rising bubbles are shown in Fig. 15 in nondimensional form as Reynolds numbers, and are compared with the theoretical terminal Reynolds numbers for spherical vapor bubbles rising in a bubbly liquid mixture, under a balance of buoyancy and drag forces. The theoretical terminal

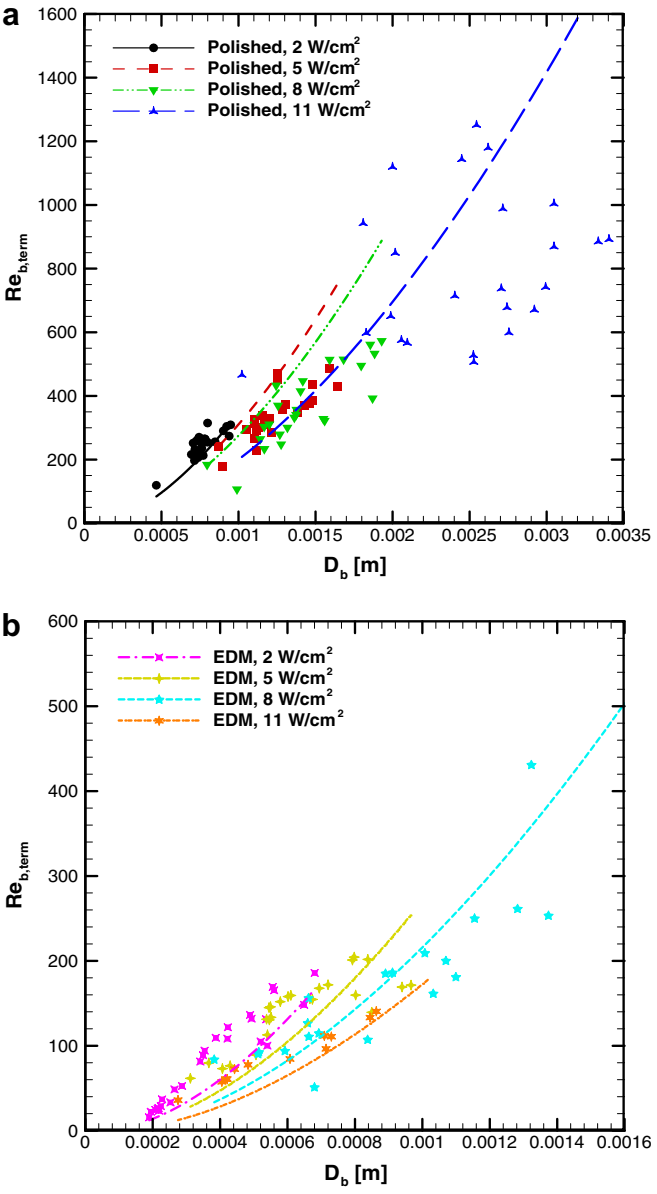

Fig. 15. Variation of bubble terminal rise Reynolds number ($Re_{b,term}$) with bubble diameter (D_b). Experimental data for (a) the polished test surface and (b) the EDM-roughened surface are plotted along with theoretical predictions from Eq. (5) through (7).

Table 3
Mean absolute error (MAE) of Ishii–Zuber viscous drag correlation (Ishii and Zuber, 1979) with respect to experimental bubble terminal Reynolds numbers.

Test case (W/cm^2)	Number of points	MAE (%)[a]	Notes
Polished, 2	26	14.5	Slightly underpredicted $Re_{b,term}$
Polished, 5	25	36.5	Overpredicted $Re_{b,term}$
Polished, 8	25	45.3	Overpredicted $Re_{b,term}$
Polished, 11	24	47.8	Overpredicted $Re_{b,term}$; error not Gaussian
EDM, 2	26	30.0	Underpredicted $Re_{b,term}$
EDM, 5	25	27.3	Slightly underpredicted $Re_{b,term}$
EDM, 8	21	29.7	Slightly overpredicted $Re_{b,term}$
EDM, 11	12	25.2	Underpredicted $Re_{b,term}$; frequent coalescences obscured velocity meas

[a] MAE is defined as the sum of the absolute deviations of the correlation with respect to the experimentally measured values, divided by the sum of the experimentally measured values.

velocity is based upon the measured bubble diameter at departure according to:

$$v_f = \dot{y}_f = \sqrt{\left(\frac{4}{3}\right)\frac{gD_d}{C_D}\left(\frac{\rho_l - \rho_v}{\rho_l}\right)}. \quad (5)$$

The theoretical drag coefficients may be evaluated with reasonable agreement according to the viscous drag correlation (Ishii and Zuber, 1979):

$$C_D = \frac{24}{\mathrm{Re}}(1 + 0.1\mathrm{Re}^{0.75}), \quad (6)$$

where the Reynolds number is the mixture-viscosity corrected value, with mixture viscosity μ_{mix} obtained by the expression:

$$\frac{\mu_{mix}}{\mu_l} = \left(1 - \frac{\alpha_v}{\alpha_{v,max}}\right)^{-2.5\alpha_{v,max}(\mu_v + 0.4\mu_l)/(\mu_v + \mu_l)}. \quad (7)$$

A number of additional terms are introduced in Eq. (7) and require further explanation. Void fraction, α_v, may attain a maximum value, $\alpha_{v,max}$, of 1. The void fraction was not measured directly, but was estimated to first order as the ratio of the evaporative component of heat flux to the evaporative component of the maximum heat flux. The evaporative component itself was estimated as the total heat flux minus the natural convection heat flux predicted for each wall superheat temperature. The resulting void fraction values were consistent with those measured for water at low, medium and high heat fluxes by Iida and Kobayasi (1969). The vapor viscosity for FC-77 is not available in the literature, but it is a reasonable assumption for most gases at atmospheric pressure to use the estimate $\mu_v \approx 2 \times 10^{-5}$ kg/m s.

In Table 3, the mean absolute error (MAE) of the Ishii–Zuber (1979) correlation with respect to the experimental data is given along with the number of experimental values included in the comparison. The observed bubble mixture Reynolds numbers ranged between 15 and 1250. The good agreement (less than 50% MAE) shows that the assumption of a quiescent pool is reasonable and that the frequent bubble interactions do not prevent the conventional two-phase drag model from being used in an averaged sense, even for rather high heat fluxes. It is worth noting that slightly better agreement could be obtained for high heat fluxes using the Newton's regime drag model proposed in (Ishii and Zuber, 1979). This model, however, is not applicable for smaller bubbles.

6. Conclusions

Important bubble nucleation parameters during the pool boiling of FC-77 on smooth and rough surfaces are experimentally investigated. The pool boiling observed was characterized by high bubble densities and numerous interactions between bubbles. The characteristics of bubble nucleation from the two surfaces at various heat fluxes were compared qualitatively. Measurements were obtained from high-speed movies for 25 individual bubbles per test case, comprised of five consecutive bubbles from each of five nucleation sites on the surface.

Bubble diameter at departure was shown to increase with increasing wall superheat, but the surface roughness was also shown to have an influence. Bubble departure frequency, which in general also increased with heat flux, was not well predicted by any of the correlations considered from the literature. Active nucleation site density was shown to increase with both wall superheat and surface roughness. Active site density was reasonably well predicted for both the polished and roughened surfaces by the Hibiki–Ishii (2003) correlation. Terminal rise velocity increased with increasing heat flux due to the increased buoyancy from larger bubble volumes; average pool boiling bubble velocities were shown to be well predicted by the Ishii–Zuber (1979) mixture-viscosity based correlation for viscous drag.

It is suggested that new bubble nucleation correlations be developed which incorporate the important effect of surface roughness, so that recent developments in mechanistic modeling can be applied for a broad range of boiling surfaces.

Acknowledgments

Financial support for this work is provided by the Indiana 21st Century Research and Technology Fund and the Cooling Technologies Research Center, a National Science Foundation Industry/University Cooperative Research Center at Purdue University. The authors acknowledge the technical insights and suggestions provided by Benjamin Jones, and thank 3 M Corporation (in particular, Phil Tuma) for providing fluid samples and related information.

References

3M Corporation, 1986. Fluorinert liquids product manual. 3M Corporation.
3M Corporation, 2000. Fluorinert electronic liquid FC-77 product information. 3M Corporation, Document 98-0212-2309-8 (HB).
Abarajith, H.S., Dhir, V.K., Warrier, G., Son, G., 2004. Numerical simulation and experimental validation of the dynamics of multiple bubble merger during pool boiling under microgravity conditions. Transport Phenomena in Microgravity 1027, 235–258.
Benjamin, R., Balakrishnan, A., 1996. Nucleate pool boiling heat transfer of pure liquids at low to moderate heat fluxes. International Journal of Heat and Mass Transfer 39, 2495–2504.
Bernardin, J.D., Mudawar, I., Walsh, C.B., Franses, E.I., 1997. Contact angle temperature dependence for water droplets on practical aluminum surfaces. International Journal of Heat and Mass Transfer 40, 1017–1033.
Bier, K., Gorenflo, D., Salem, M., Tanes, Y., 1979. Effect of pressure and surface roughness on pool boiling of refrigerants. International Journal of Refrigeration 2, 211–219.
Borishanskiy, V., Danilova, G., Gotovskiy, M., Borishanskiy, A., Danilova, G., Kupriyanova, A., 1981. Correlation of data on heat transfer in and elementary characteristics of the nucleate boiling mechanism. Heat Transfer – Soviet Research 13, 100–116.
Chekanov, V., 1977. Interaction of centers during nucleate boiling. Teplofizika Vysokikh Temperature 15, 121–128.

Cole, R., 1967. Frequency and departure diameter at sub-atmospheric pressures. American Institute of Chemical Engineers Journal 13, 779–783.
Cole, R., Rohsenow, W., 1969. Correlation of bubble departure diameters for boiling of saturated liquids. Chemical Engineering Progress Symposium Series 65, 211–213.
Cole, R., Shulman, H.L., 1966. Bubble departure diameters at subatmospheric pressures. Chemical Engineering Progress 62, 6–16.
Cornwell, K., 1982. On boiling incipience due to contact-angle hysteresis. International Journal of Heat and Mass Transfer 25, 205–211.
Darby, R., 1964. The dynamics of vapour bubbles in nucleate boiling. Chemical Engineering Science 19, 39–49.
Forster, H., Greif, R., 1959. Heat transfer to a boiling liquid: mechanism and correlations. Journal of Heat Transfer 81, 43–53.
Forster, H.K., Zuber, N., 1955. Dynamics of vapor bubbles and boiling heat transfer. American Institute of Chemical Engineers Journal 1, 531–535.
Fritz, W., 1935. Berechnung des maximalvolume von dampfblasen. Physikalische Zeitschrift 36, 379–388.
Gorenflo, D., Danger, E., Luke, A., Kotthoff, S., Chandra, U., Ranganayakulu, C., 2004. Bubble formation with pool boiling on tubes with or without basic surface modifications for enhancement. International Journal of Heat and Fluid Flow 25, 288–297.
Han, C., Griffith, P., 1965. The mechanism of heat transfer in nucleate boiling. Parts I and II. International Journal of Heat and Mass Transfer 8, 887–914.
Hatton, A., Hall, I., 1966. Photographic study of boiling on prepared surfaces. In: Proceedings of 3rd International Heat Transfer Conference, vol. 4. pp. 24–37.
Hazi, G., Markus, A., 2009. On the bubble departure diameter and release frequency based on numerical simulation results. International Journal of Heat and Mass Transfer 52, 1472–1480.
Hendricks, R., Sharp, R., 1964. Initiation of cooling due to bubble growth on a heating surface. National Aeronautics and Space Administration Lewis Research Center, TN D-2290, report no. TN D-2290.
Hibiki, T., Ishii, M., 2003. Active nucleation site density in boiling systems. International Journal of Heat and Mass Transfer 46, 2587–2601.
Hong, K.T., Imadojemu, H., Webb, R.L., 1994. Effects of oxidation and surface roughness on contact angle. Experimental Thermal and Fluid Science 8, 279–285.
Hsu, Y.Y., 1962. On the size range of active nucleation cavities in a heating surface. Journal of Heat Transfer 84, 207–216.
Hsu, Y., Graham, R.W., 1961. An analytical and experimental study of the thermal boundary layer and ebullition cycle in nucleate boiling. National Aeronautics and Space Administration Lewis Research Center, NASA-TN-D-594, report no. NASA-TN-D-594.
Iida, Y., Kobayasi, K., 1969. Distributions of void fraction above a horizontal heating surface in pool boiling. Bulletin of JSME 12, 283–290.
Ishii, M., Zuber, N., 1979. Drag coefficient and relative velocity in bubbly, droplet or particulate flows. AIChE Journal 25, 843–855.
Jakob, M., Fritz, W., 1931. Versuche über den verdampfungsvorgang. Forschung auf dem Gebiete des Ingenieurwesens 2, 435–447.
Jensen, M.K., Memmel, G.J., 1986. Evaluation of bubble departure diameter correlations. In: Proceedings of the Eighth International Heat Transfer Conference, vol. 4. pp. 1907–1912.
Jones, B.J., Garimella, S.V., 2007. Effects of surface roughness on the pool boiling of water. In: 2007 Proceedings of the 5th Joint ASME/JSME Fluids Engineering Conference, paper no. HT 2007-32230.
Jones, B.J., McHale, J.P., Garimella, S.V., 2009. The influence of surface roughness on nucleate pool boiling hea transfer. Journal of Heat Transfer 131, 121009. doi:10.1115/1.3220144.
Judd, R., Hwang, K., 1976. A comprehensive model for nucleate pool boiling heat transfer including microlayer evaporation. Journal of Heat Transfer 98, 623–629.
Kandlikar, S.G., Steinke, M.E., 2001. Contact angles of droplets during spread and recoil after impinging on a heated surface. Chemical Engineering Research and Design 79, 491–498.
Kandlikar, S.G., Steinke, M.E., 2002. Contact angles and interface behavior during rapid evaporation of liquid on a heated surface. International Journal of Heat and Mass Transfer 45, 3771–3780.
Kim, J., Oh, B.D., Kim, M.H., 2006. Experimental study of pool temperature effects on nucleate pool boiling. International Journal of Multiphase Flow 32, 208–231.
Kolev, N.I., 1995. How accurately can we predict nucleate boiling? Experimental Thermal and Fluid Science 10, 370–378.
Kotthoff, S., Gorenflo, D., 2009. H e a t transfer and bubble formation on horizontal copper tubes with different diameters and roughness structures. Heat and Mass Transfer 45, 893–908.
Kutateladze, S., Gogonin, I., 1980. Growth rate and detachment diameter of a vapor bubble in free convection boiling of a saturated liquid. High Temperature 17, 667–671.
Lee, H.C., Oh, B.D., Bae, S.W., Kim, M.H., 2003. Single bubble growth in saturated pool boiling on a constant wall temperature surface. International Journal of Multiphase Flow 29, 1857–1874.
Lord Rayleigh, 1917. On the pressure developed in a liquid during the collapse of a spherical bubble. Philosophical Magazine 34, 94–98.
Lorenz, J.J., Mikic, B.B., Robsenow, W.M., 1974. Effect of surface conditions on boiling characteristics. In: Proceedings of 5th International Heat Transfer Conference, vol. 4. Hemisphere, New York, pp. 35–39.
Luke, A., 2003. Thermo- and fluid dynamic in boiling – connection between surface roughness, bubble formation and heat transfer. In: Proceedings of 5th international conference on boiling heat transfer, 20030504-08.
Luke, A., 2009. Preparation and analysis of different roughness structures for evaporator tubes. Heat and Mass Transfer 45, 909–917.
Luke, A., Baumhogger, E., Scheunemann, P., 2000. 3-dimensional description of the microstructure of heated surfaces in nucleate pool boiling. Multiphase Science & Technology 12, 136–151.
McHale, J.P., Garimella, S.V., 2008. Measurements of bubble nucleation characteristics in pool boiling of a wetting liquid on smooth and roughened surfaces. In: Proceedings of 2008 ASME Summer Heat Transfer Conference, paper no. HT 2008-56179.
Michaelides, E., 2003. Hydrodynamic force and heat/mass transfer from particles, bubbles, and drops – the freeman scholar lecture. Journal of Fluids Engineering 125, 209–238.
Mikic, B.B., Rohsenow, W.M., 1969a. Bubble growth rates in non-uniform temperature field. Progress in Heat and Mass Transfer 2, 283–293.
Mikic, B.B., Rohsenow, W.M., 1969b. A new correlation of pool-boiling data including the effect of heating surface characteristics. Journal of Heat Transfer 91, 245–250.
Mikic, B.B., Rohsenow, W.M., Griffith, P., 1970. On bubble growth rates. International Journal of Heat and Mass Transfer 13, 657–666.
Moghaddam, S., Kiger, K., 2009. Physical mechanisms of heat transfer during single bubble nucleate boiling of FC-72 under saturation conditions. II: theoretical analysis. International Journal of Heat and Mass Transfer 52, 1295–1303.
Peebles, F.N., Garber, H.J., 1953. Studies on motion of gas bubbles in liquids. Chemical Engineering Progress 49, 88–97.
Pinto, A.D., Gorenflo, D., Kunstler, W., 1996. Heat transfer and bubble formation with pool boiling of propane at a horizontal copper tube. In: Proceedings of 2nd European Thermal Science and 14th UIT National Heat Transfer Conference, vol. 2. pp. 1653–1660.
Qi, Y., Klausner, J.F., 2005. Heterogeneous nucleation with artificial cavities. Journal of Heat Transfer 127, 1189–1196.
Rohsenow, W.M., 1952. A method of correlating heat transfer data for surface boiling of liquids. Transactions of the ASME 74, 969–976.
Ruckenstein, E., 1961. A physical model for nucleate boiling heat transfer from a horizontal surface. Buletinul Institutului Politehnic Bucuresti (Romania) 23, 79–88.
Sultan, M., Judd, R., 1983. Interaction of the nucleation phenomena at adjacent sites in nucleate boiling. Journal of Heat Transfer 105, 3–9.
Tien, C.L., 1962. A hydrodynamic model for nucleate pool boiling. International Journal of Heat and Mass Transfer 5, 533–540.
Tong, W., Bar-Cohen, A., Simon, T.W., You, S.M., 1990. Contact angle effects on boiling incipience of highly-wetting liquids. International Journal of Heat and Mass Transfer 33, 91–103.
Van Stralen, S., 1970. The boiling paradox in binary liquid mixtures. Chemical Engineering Science 25, 149–171.
Wang, C.H., Dhir, V.K., 1993a. Effect of surface wettability on active nucleation site density during pool boiling of saturated water. Journal of Heat Transfer 115, 659–669.
Wang, C.H., Dhir, V.K., 1993b. On the gas entrapment and nucleation site density during pool boiling of saturated water. Journal of Heat Transfer 115, 670–679.
Zhang, L., Shoji, M., 2003. Nucleation site interaction in pool boiling on the artificial surface. International Journal of Heat and Mass Transfer 46, 513–522.
Zuber, N., 1963. Nucleate boiling-the region of isolated bubbles-similarity with natural convection. International Journal of Heat and Mass Transfer 6, 53–65.